Mechanochemical Synthesis as a Greener Way to Produce Iron-based Oxygen Reduction Catalysts

M. Gernhard,*[a] M. Rautenberg,[b, c] G. Hörner,[d] B. Weber,[d] F. Emmerling,[b, c] and C. Roth[a]

Dedicated to Professor Josef Breu on the occasion of his 60th birthday

Iron-based catalysts have been reported manifold and studied as platinum group metal (PGM) free alternatives for the catalysis of the oxygen reduction reaction (ORR). However, their sustainable preparation by greener synthesis approaches is usually not discussed. In this work, we propose a new method for the sustainable preparation of such catalysts by using a mechanochemical approach, with no solvents and non-toxic chemicals. The materials obtained from low temperature carbonization (700 °C) exhibit considerable and stable catalytic performance for ORR in alkaline medium. A catalyst obtained from iron hydroxide, tryptophan, dicyandiamide, and ammonium nitrate shows the best electrocatalytic performance with an overpotential of 921 mV vs. RHE at 0.1 mA/cm^2 and an electron transfer number of 3.4.

1. Introduction

With widespread utilization of renewable energy resources such as wind and solar energy the need to adjust for peak loads becomes a bottleneck for the continuous supply with energy.[1] Furthermore, an increasing number of electrical vehicles will likely become a challenge soon, as their batteries will be charged around the same time when people get home from work resulting in unknown peak loads.[2] Therefore, highly efficient energy storage and conversion devices are urgently sought after.[3] Promising technologies such as fuel cells and metal air batteries often rely on the electrocatalytic reduction of oxygen e.g. from air supplied at the cathode. The sluggish ORR is usually facilitated by expensive precious metal catalysts – most commonly platinum group metals (PGM).[4,5] Besides the fact that these rare metals are a major cost driver,[6] industry is also held back due to the risk of shortages when demands increase or geopolitical crisis strikes one of the few producing and exporting countries.[7] Therefore, various PGM-free catalysts have been developed over the past decades.[8–11] Iron-based catalysts are among the most promising PGM-free catalysts with performances comparable to PGM catalysts under alkaline conditions.[12,13] In acidic electrolyte, however, Fe-based catalysts form hydrogen peroxide that in the presence of iron ions can degrade the ionomer.[8,10] Hence, one use case for Fe-based catalysts is most likely in anion exchange membrane fuel cells (AEMFCs) and metal air batteries.[12–17] Exactly how these catalyse the ORR is still under debate, and multiple catalytic sites have been proposed over the years, since the first iron-based catalysts were prepared by Jasinski in 1964.[18] Fe–N$_4$ sites embedded in a carbon matrix and similar structures with Fe–N$_x$ stoichiometries are usually referred to as Fe–N–C type catalysts. Many efforts have been undertaken to prepare atomically dispersed Fe–N–C type catalysts to allow for a detailed study of their mechanism.[19–21] Some studies that take DFT calculations into consideration suggest that O$_2$ binds to the Fe single atom centre where it is reduced to water via a 4-electron pathway.[22] Other groups proposed that metal ions only have a directing effect in the formation of ORR active nitrogen doped graphitic materials.[23] However, in both cases the outstanding activity can only be explained by considering the metal centres as main contributing active sites. A few studies have furthermore shown that carbon encapsulated Fe$_3$C nanoparticles may also act as ORR active sites yielding electrocatalysts with promising performances.[24] The catalytic mechanism of this type of catalysts is still under investigation.[25]

Fe-based catalysts are often prepared by the carbonization of suitable precursors under inert conditions. Many different synthetic routes for such precursors have proven successful in the past, for example MOF based precursors such as MIL-101.[17,24] Other authors prepared tar-like precursors from polyaniline and iron chloride[22,26] or used pig blood from slaughterhouses.[27] Alternative green methods of synthesizing Fe–N–C type catalysts actually require hazardous chemicals like

[a] *M. Gernhard, C. Roth*
Chair of Electrochemical Process Engineering
Universität Bayreuth
Universitätsstraße 30, 95447 Bayreuth, Germany
E-mail: gernhard@uni-bayreuth.de

[b] *M. Rautenberg, F. Emmerling*
BAM Federal Institute of Materials Research and Testing
Richard-Willstätter-Str. 11, 12489 Berlin, Germany

[c] *M. Rautenberg, F. Emmerling*
Department of Chemistry
Humboldt-Universität zu Berlin
Brook-Taylor-Str. 2, 12489 Berlin, Germany

[d] *G. Hörner, B. Weber*
Department of Chemistry
Universität Bayreuth
Universitätsstraße 30, 95447 Bayreuth, Germany

CTAB and 2-methylimidazole[28] or energy intensive methods like autoclaving and freeze drying.[29] One thing all proposed syntheses – even though termed "green" – have in common is the use of solvents.

Herein, we propose a synthetic route that uses no solvents, a more energy efficient temperature profile and only non-toxic chemicals. As an iron source, we substituted ferric chloride by iron hydroxide as a more abundant and less corrosive material. Tryptophan was used as major carbon and nitrogen source for its non-hazardous character and its availability from plants, such as spirulina and soybeans.[30] Cyanamide was used in previous studies as pore directing agent, but is toxic to humans. Dicyandiamide (DCD) was therefore used as a non-toxic alternative showing very similar physicochemical properties. Instead of common lengthy autoclave reactions or solvent evaporation methods we used a mechanochemical approach with no solvents. This approach has been previously reported as a cleaner synthetic route towards metal organic frameworks.[31,32] Being the first to use this approach, we were able to decrease reaction times down to one hour and produced no solvent waste during the precursor preparation. The precursors were then carbonized for 1 h at 700 °C, which is the most energy efficient temperature profile compared to the reported procedure of 900 °C for at least 1 h, which is carried out twice to enhance the graphitization degree of the resulting material. At these low carbonization temperatures, however, electrical conductivity and percolation between the catalytical centres and the rest of the electrode can become an issue. Therefore, we also studied the effect of adding small amounts of conductive Vulcan carbon (VC) to the precursor expecting to thereby increase the overall performance of the catalyst. We tested the materials performance for the ORR in alkaline conditions aiming for high activity.

Experimental Section

Reagents and Methods

The hydrate form of iron (III) oxide hydroxide will be referred to as iron trihydroxide and was freshly prepared in a typical aqueous precipitation approach from ferric chloride and ammonia solution.[33] Ferric chloride (*Sigma Aldrich*), ammonia solution (*Brand*), 1-cyanoguanidine (*Merck*), Vulcan Carbon VXC 72R (*Quintech*; LOT: 4687250) and ammonium nitrate (*Merck*) were obtained from commercial suppliers in analytical grade. Tryptophan was obtained from *bulk* (*formerly bulk powders*) in food grade. All chemicals were used without further purification. Water was used from a MilliQ system with a specific conductivity of >18 MΩcm.

Powder X-Ray Diffraction

Reaction products of the ball milling process and carbonization procedure were identified via Powder X-ray diffraction (PXRD). This was recorded on a *Bruker D8 Advance* X-ray diffractometer in a Bragg-Brentano geometry with a Lynxex-detector using Cu-K$_{\alpha}$1 radiation ($\lambda = 1.540566$ Å). Diffraction patterns were acquired in a scanning range from 5° to 80° 2θ, at 0.02° step size. The time per step was 0.6 s. Therefore, the as-synthesized precursors and catalyst powders were placed in PVC sample holders. Recorded diffracto-grams were evaluated using *X'Pert HighScore* software from *Malvern Panalytical*.[34]

Thermogravimetric Analysis

Thermogravimetric analysis (TGA) was used to find the lowest possible carbonization temperature of the precursors and for the subsequent controlled carbonization thereof. TGA was performed on a *Netzsch STA 449 F5 Jupiter* using 0.8 ml Al$_2$O$_3$ crucibles at a heating rate of 2.5 K/min in an N$_2$ atmosphere. Approximately 20 mg of the as synthesized precursor powders were used for the surveys and 40 mg for the carbonization obtaining the catalysts. The proprietary Software *Proteus* from *Netzsch* was used for data evaluation.

Transmission Electron Microscopy

The surface morphology of catalyst materials before and after accelerated stress tests as well as the structure identification of essential features were evaluated by transmission electron microscopy (TEM). TEM images were recorded with a *JEOL JEM-2200FS* energy filtered transmission electron microscope at 200 kV using a CMOS camera with *Digital Micrograph* software (*Digital Micrograph 3.9, Gatan*). Images were recorded of the scraped-of thin films from ink drop casted glassy carbon electrodes (GC). These were dispersed in hexanes and drop casted onto lacey carbon coated copper grids.

^{57}Fe Mössbauer Spectroscopy

Room temperature Mössbauer spectroscopy was performed to identify iron species present before and after carbonization of the precursors. Mössbauer spectra were recorded in transmission geometry in a constant acceleration mode using a conventional Mössbauer spectrometer equipped with a 50 mCi57Co(Rh) source. The as-synthesized precursor and catalyst were used and resulting spectra fitted using Recoil 1.05 Software with α-iron as standard.[35]

Porosimetry

Brunauer-Emmett-Teller (BET) specific surface areas and pore size distributions using the Barrett, Joyner, and Halenda (BJH) method were measured with a *Micromeritics ASAP (Accelerated Surface Area and Porosimetry system) 2010*. 1 g of the samples were degassed for several hours at 80 °C in high vacuum prior to measurements to remove water and other surface contaminants. The temperature was chosen so that no decomposition would take place as indicated by TGA measurements.

All data were plotted in OriginLab Origin 2021 Version 9.8.0.200.

Synthesis of Fe-based Electrocatalysts

The Fe-Trp precursors were synthesized by a mechanochemical approach without any solvents according to Table 1. For this purpose, the reactants were placed in a ball mill bomb with 20 g (approx. 60 pcs) of CrMnFe steel balls. Soluble salts can be added to the reaction mixture prior to the milling process as salt matrices that facilitate an agglomeration-free product.[36] In our study, we added ammonium nitrate as an agglomeration inhibitor. Without the need of washing the precursor product, ammonium nitrate should decompose during the carbonization step and possibly also has a positive influence on the nitrogen content in the catalyst material. The bomb was then placed in a planetary ball mill

Table 1. Precursor reaction mixtures [weights in mg (equivalents with respect to $Fe(OH)_3$)].

Sample	$Fe(OH)_3$	Trp	DCD	VC	NH_4NO_3
Fe-Trp	110.60	406.63 (1.92)	–	–	16.73 (0.20)
Fe-Trp +DCD	105.00	409.46 (2.04)	19.19 (0.23)	–	16,35 (0.21)
Fe-Trp+VC	106.49	404.37 (1.99)	–	32.24 (5.7)[a]	19.29 (0.24)
Fe-Trp +DCD+VC	107.28	405.75 (1.98)	17.36 (0.21)	31.58 (5.5)[a]	16.15 (0.20)

[a] weight-% with respect to $Fe(OH)_3$.

(Pulverisette 5, Fritsch, Germany) and rotated at 250 rpm for 1 h. The steel balls were then removed, and the obtained powders used without further purification.

Fe-based electrocatalysts were obtained by one-step carbonization of Fe-Trp precursors at 700 °C at a rate of 2.5 K/min in an N_2 atmosphere. The temperature was held for 1 h and then allowed to cool down to room temperature.

Electrochemical Measurements

Electrochemical measurements were performed by thin-film rotating disk electrode measurements with a *Biologic VSP-300* Potentiostat using a three-electrode cell setup. Carbon felt (30 x 10 x 5 mm³) on a glassy carbon (GC) rod was used as counter electrode and Ag/AgCl (3 M KCl) as reference electrode with a constant potential of 206 mV vs. SHE checked before and after each experiment. The 0.1 M KOH electrolyte was kept at a constant temperature of 25.0 °C using a thermostat and mantled cell. The GC rotating disk electrode (RDE) tips were manufactured in-house and used with a *Metrohm Autolab* RDE setup. Prior to loading the GC RDE tip with catalyst ink the tip was polished with 1 and 0.05 μm alumina slurry (*MicroPolish II and MasterPrep, Buehler*) and washed in MilliQ water in an ultrasonic bath for 5 min. The inks were prepared by weighing in 5.00 mg of catalyst material and adding
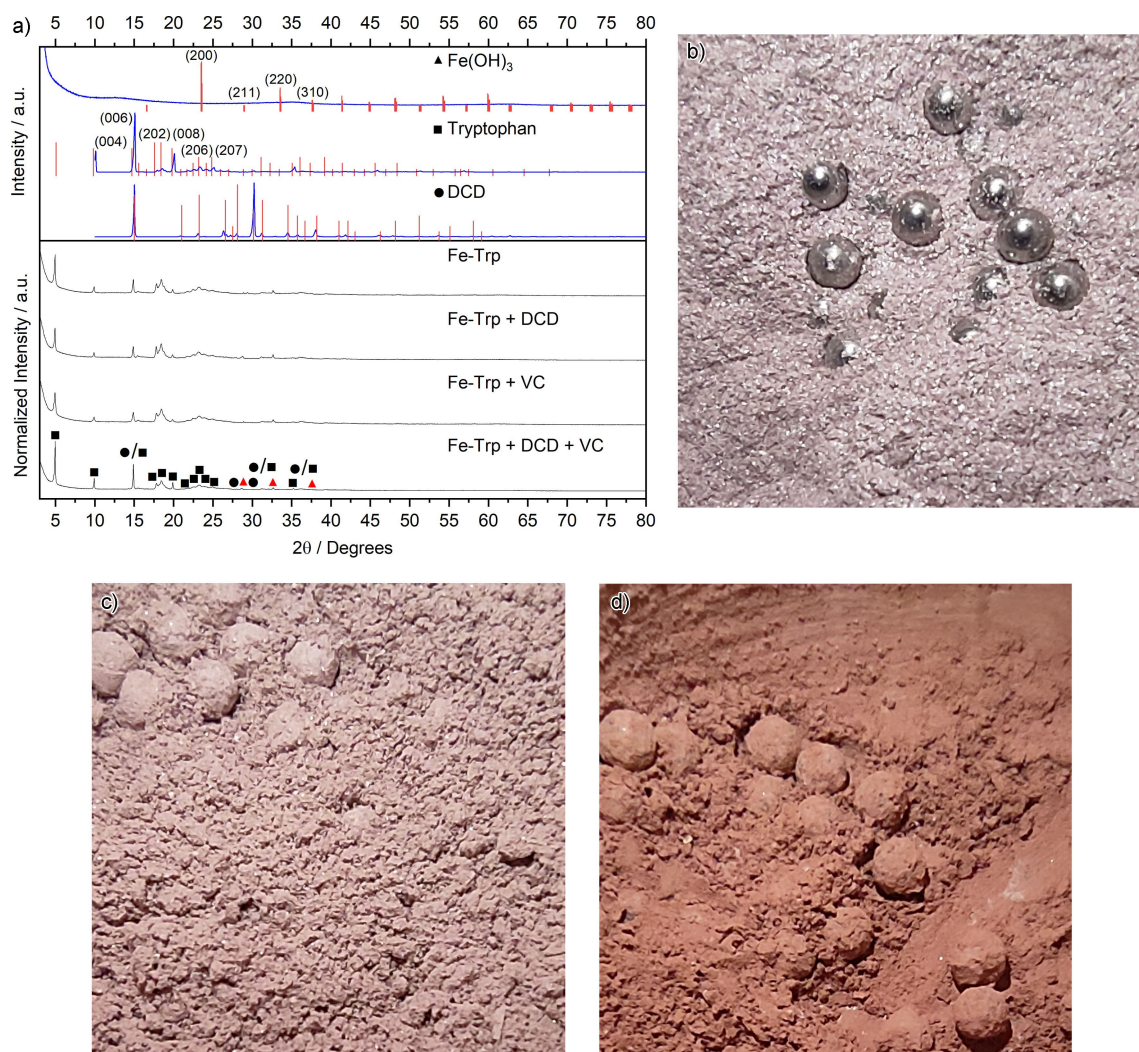

Figure 1. (a) PXRD of reactants (blue), their reference diffractograms (red), and reaction mixtures (black) after 60 min ball milling, where symbols (■: Trp, ●: DCD, ▲: $Fe(OH)_3$) denote reflections of the respective reactant (red if reflection appeared); (b) images of the reaction mixture of Fe-Trp+DCD before, after 5 min (c), and after 60 min of ball milling (d).

1.000 ml of a solution of DMF:H$_2$O (50 ml:50 ml + 0.8 ml *Nafion D2021*). The ink was dispersed by first sonicating in a *Bandelin sonorex super* ultrasonic bath for 30 min at 35 kHz and subsequently at 30 kHz for 30 s (50% duty cycle) with a *Bandelin sonoplus mini20* ultrasonic homogenizer. Immediately after the sonication procedure a drop of 20 µl ink was placed on the 7 mm diameter GC RDE tip to obtain a catalyst loading of 260 µg/cm^2. The solvent was then evaporated under vacuum and the film checked for uniformity under a stereo microscope.

CVs were recorded with a scan rate of 10 mV/s at different rotation rates in the O$_2$ saturated electrolyte, measurements were repeated three times at each rotation rate to check reproducibility. The latter cathodic sweep was used for evaluation.

The electron transfer number was calculated from Levich plots.

$$j_M^{-1} = j_K^{-1} + j_L^{-1} = j_K^{-1} + B_L^{-1}\ \omega^{-0.5}$$

$$B_L = 0.62nFC_0(D_0)^{2/3}\nu^{-1/6}$$

Where j_M is the measured current density, j_K the kinetic current density and j_L the limiting current density. ω is the angular velocity of the RDE, n the electron transfer number, F is the Faraday constant, C_0 the bulk concentration of O$_2$, D_0 the diffusion coefficient of O$_2$ in the electrolyte and ν the kinematic viscosity of the electrolyte.

2. Results and Discussion

The solvent-free mechanochemical approach yielded a crystalline precursor material which is mainly composed of the reactants as can be derived from the PXRD in Figure 1a. While the (006) and (008) reflections of tryptophan (ICDD-00-025-1960) appear unchanged in the diffraction pattern of Fe-Trp, the (202), (206), and (207) reflections are more intense after the milling process. The PXRD of the Fe(OH)$_3$ shows two very broad reflections, as is expected for iron oxide hydroxides that are obtained as voluminous precipitates. The difficulty in characterizing iron trihydroxide prepared from the hydrolysis of Fe^{3+} in basic solution is well known.[38] These broad features from the amorphous Fe(OH)3 are present in the diffractograms of all precursors. However, some additional reflections appear after the milling process, that might be assigned to the (211), (220), and (310) reflections of crystalline iron trihydroxide as indicated by the simulated PXRD from crystallographic data of iron trihydroxide.[39] Other reflections, like the (200) reflection of iron trihydroxide that overlaps with the (206) reflection of tryptophan and the (111) reflection of dicyandiamide (ICDD-00-011-0703) at around 23° 2θ, cannot be unambiguously assigned. It remains unclear whether the observed color change of the reaction mixture shown in Figure 1b–d originates from the crystallization of the iron trihydroxide or from the finer dispersion of the reactants after milling. Interestingly, the addition of neither Vulcan carbon (VC), nor dicyandiamide (DCD) seems to have an impact on the precursor material, as the diffraction patterns remain unchanged. Overall, the PXRDs indicate, that the anticipated reaction of iron trihydroxide with tryptophan did not take place.

The thermogravimetric analysis (TGA) in Figure 2a shows that all precursors behave similarly during carbonization in a nitrogen atmosphere and have undergone mass loss associated complete decomposition at 660 °C. As expected, the precursors containing VC show a smaller mass loss, since VC will not undergo decomposition under the applied conditions. Only the precursor without VC and DCD showed an additional peak in the first differential of the TG at 580 °C and a small change at 1350 °C. Even though graphitization will most likely be facilitated at higher temperatures of >900 °C, carbonization at 700 °C should result in the formation of the sought-after catalytic sites. Mass losses below 200 °C are associated to liberation of water with no significant influence on the catalyst.

In the PXRD of the resulting catalysts shown in Figure 2b an amorphous structure can be derived from the very broad reflection at around 25° 2θ that most likely results from porous carbon. The reflection pattern between 30° and 50° 2θ can be assigned to iron carbide (ICDD: 03-065-2413). Using the Scherrer
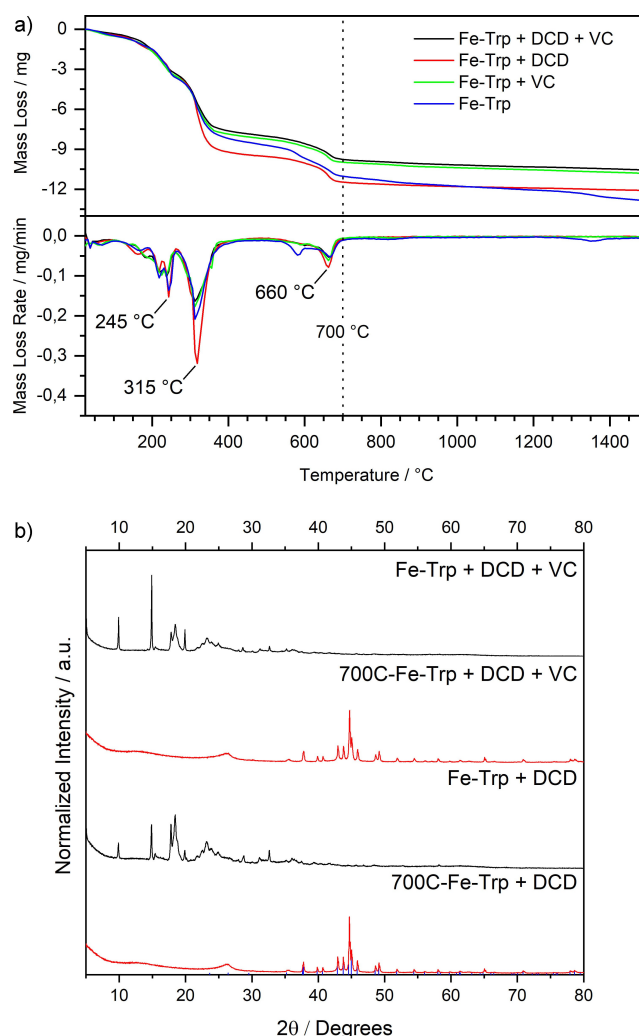

Figure 2. (a) TGA (top) and corresponding DTG (bottom) of precursors in N$_2$ between 30 and 1500 °C; (b) PXRD of catalysts (red) with their respective precursors above (black) and iron carbide reflections (ICDD-03-065-2413; blue).

equation and the FWHM of the (211) reflection at 42.98° 2θ the average crystallite size can be estimated to approximately 54 nm.

The TEM image in Figure 3a shows particles as dark spots dispersed within a cluster of porous carbon. Figure 3b shows that the distance between features in these dark particles is 2.1 ± 0.1 Å which can be assigned to the (210) plane of iron carbide. The estimated particle size of the iron carbide from PXRD also matches with the particles shown in these images. Upon further inspection one can see in Figure 3b that the Fe_3C particles are wrapped inside the typical turbostratic, onion-like structure of largely amorphous carbon.

In order to further investigate the chemical environment of iron in the precursors and in the final catalysts, room temperature ^{57}Fe-Mössbauer analyses were performed (Figure 4). The Mössbauer spectrum of the precursor, shown in Figure 4a, exhibits only one doublet, with an isomer shift $\delta = -0.339$ mm s^{-1} and a quadrupole splitting of $\Delta E_Q = 0.677$ mm s^{-1}, indicating the occurrence of single iron species (high spin Fe^{III}). There is no indication of the presence of significant amounts of other iron containing phases.

Figure 4 b presents the Mössbauer spectrum of the resulting catalyst 700C-Fe-Trp+DCD after pyrolysis at 700 °C. The recorded signal is dominated by a magnetically split sextet ($\delta = -0.190$ mm s^{-1}, $\Delta E_M = 1.422$ mm s^{-1}). The fit parameters are in good agreement with data reported for iron carbide, Θ-Fe$_3$C.[40] Signals indicating minor contributions of an additional magnetically split signal with somewhat larger quadrupole splitting are observed at $v = \pm 5.3$ mm s^{-1}. The composite analysis of the experimental data to two sextets gave no statistically stable fit.

An overall similar picture prevails for the catalyst 700C-Fe-Trp as shown in Figure 4c. Again, the recorded signal is dominated by a magnetically split sextet ($\delta = -0.191$ mm s^{-1}, $\Delta E_M = 1.421$ mm s^{-1}). The close match among the fit parameters of both catalysts may indicate a largely conserved chemical environment of iron in both materials. It is noted, however, that the contribution of the minor component, which appears in both spectra, is significantly stronger in 700C-Fe-Trp. It has been shown in the literature, that many different components can be formed during the carbonization of iron-based materials, and it comes as no surprise, that there is a contribution of minor components visible in both carbonized precursors.[41] The composite analysis of the experimental data of 700C-Fe-Trp to two sextets gave no statistically stable fit; nevertheless, an isomeric shift δ close to zero and a quadrupole splitting of $\Delta E_M = 2.24$ mm s^{-1} may be taken as a valid guess.

Nitrogen adsorption-desorption isotherms of Fe-Trp+DCD before and after carbonization are shown in Figure 5. From these an increase of the BET specific surface area from 4.4 m^2/g to 266 m^2/g can be derived. While the surface area increase is significant, the absolute surface area is still small compared to activated carbon materials that are for example used in the preparation of platinum-based catalysts or can be obtained from metal organic framework precursors. Furthermore, the average BJH adsorption pore diameter decreases from 161.8 Å before carbonization to 58.8 Å after heat-treatment.

The onset potential of an electrocatalyst is considered a suitable measure for its catalytic activity, as it depends on the overpotential that is needed to drive a reaction. Hence, the lower the overpotential, the more active the catalyst.[42] The region just negative of the onset potential is controlled both by the kinetics of the reaction as well as the mass transport of reactants, i.e. O$_2$. The half-wave potential is therefore a measure of the steepness of this mixed controlled region and appears the closer to the onset potential the more active the catalyst. Once the overpotential is high enough to completely overcome kinetic limitations, only the mass transport limits the measured current density. This is reflected by a plateau whose current density depends on, inter alia, rotation rate of the working electrode and the number of electrons transferred in the reaction. Pt-based catalysts usually show steep mixed control regions and a well-defined plateau in the mass transport limitation region. PGM-free catalysts, however, show lower catalytic activity and therefore not necessarily a distinct plateau.
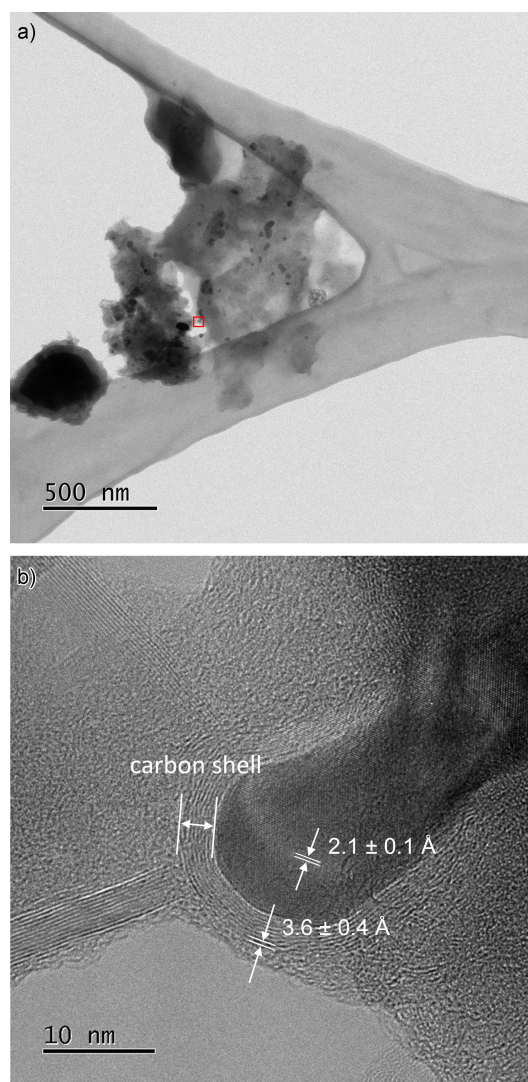

Figure 3. TEM Images of 700C-Fe-Trp+DCD; Red box showing the position of (b) within (a).
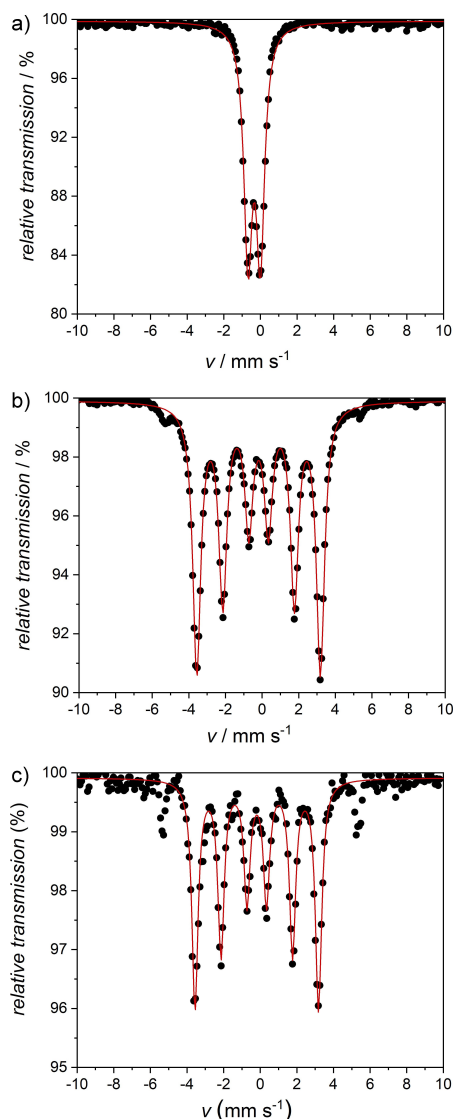
Figure 4. ^{57}Fe-Mössbauer spectrum obtained from (a) precursor Fe-Trp + DCD, (b) catalyst 700C-Fe-Trp + DCD, and (c) catalyst 700C-Fe-Trp; symbols: experimental; line: fit.

expected, as the additions should contribute extra electron conductivity increasing the overall performance. The addition of DCD on the other hand seems to slightly increase performance with respect to limiting current and – in the case of VC free precursors – onset potential. 700C-Fe-Trp + DCD showed the best performance overall with an electron transfer number of 3.4. While electron transfer numbers for Fe−N−C based catalyst can reach > 3.95,[22] our catalyst performs very well amongst other iron carbide based catalysts with transfer numbers usually ranging between 2.0 and 3.1.[25,45] The electron transfer numbers were obtained from Levich plots through RDE measurements at different rotation rates as shown in Figure 6b. The electron transfer number helps to discriminate between the unwanted indirect 2 e$^-$ mechanism toward H$_2$O$_2$ and the intended direct 4 e$^-$ mechanism. For lower binding energies of the [M]-OOH* transition state the formation of hydrogen peroxide becomes favorable.[19] This side reaction is undesired as the formation of hydrogen peroxide from oxygen follows a 2-electron pathway. The reduction to water on the other hand is a 4-electron reaction and more desirable, as higher currents and therefore power densities can be achieved. The ORR mechanism for Pt-
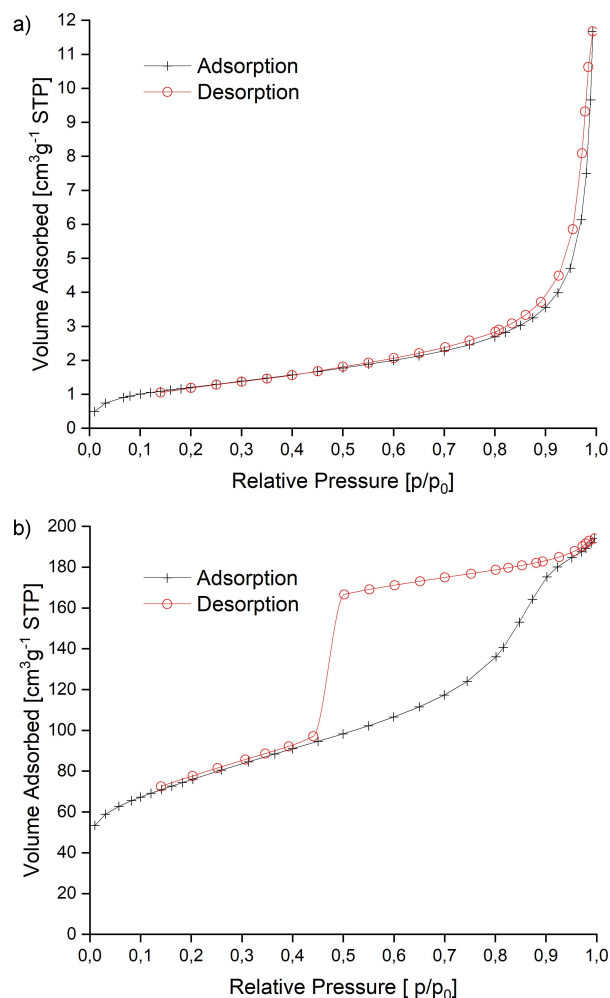

Figure 5. N$_2$ adsorption-desorption isotherm of Fe-Trp + DCD before (a) and after (b) carbonization; symbols: experimental; line: fit.

Typically, the onset potential of iron-based catalysts for the ORR in alkaline media is between 0.75 V and 0.95 V vs. RHE, while the half-wave potential can vary between 0.6 V and 0.8 V vs RHE. Limiting currents are reported between 2 mA cm^{-2} and 6 mA cm^{-2} at 1600 rpm.[22,43,44]

All prepared catalysts are ORR active in 0.1 M KOH. While onset potentials only vary between −129 mV vs. Ag/AgCl (700C-Fe-Trp) and −52 mV vs. Ag/AgCl (700C-Fe-Trp + DCD) at 100 μA/cm^2, their limiting currents vary significantly between −2.07 and −2.87 mA/cm^2 at 1600 RPM as shown in Figure 6a. The addition of VC to the precursors containing DCD results in worse performance in terms of electron transfer number (Figure 6d) as well as onset and half-wave potential (Figure 6c). With the inferior performance of the catalysts prepared without DCD the addition of VC does not seem to have any significant impact on the electrocatalytic performance. This has not been
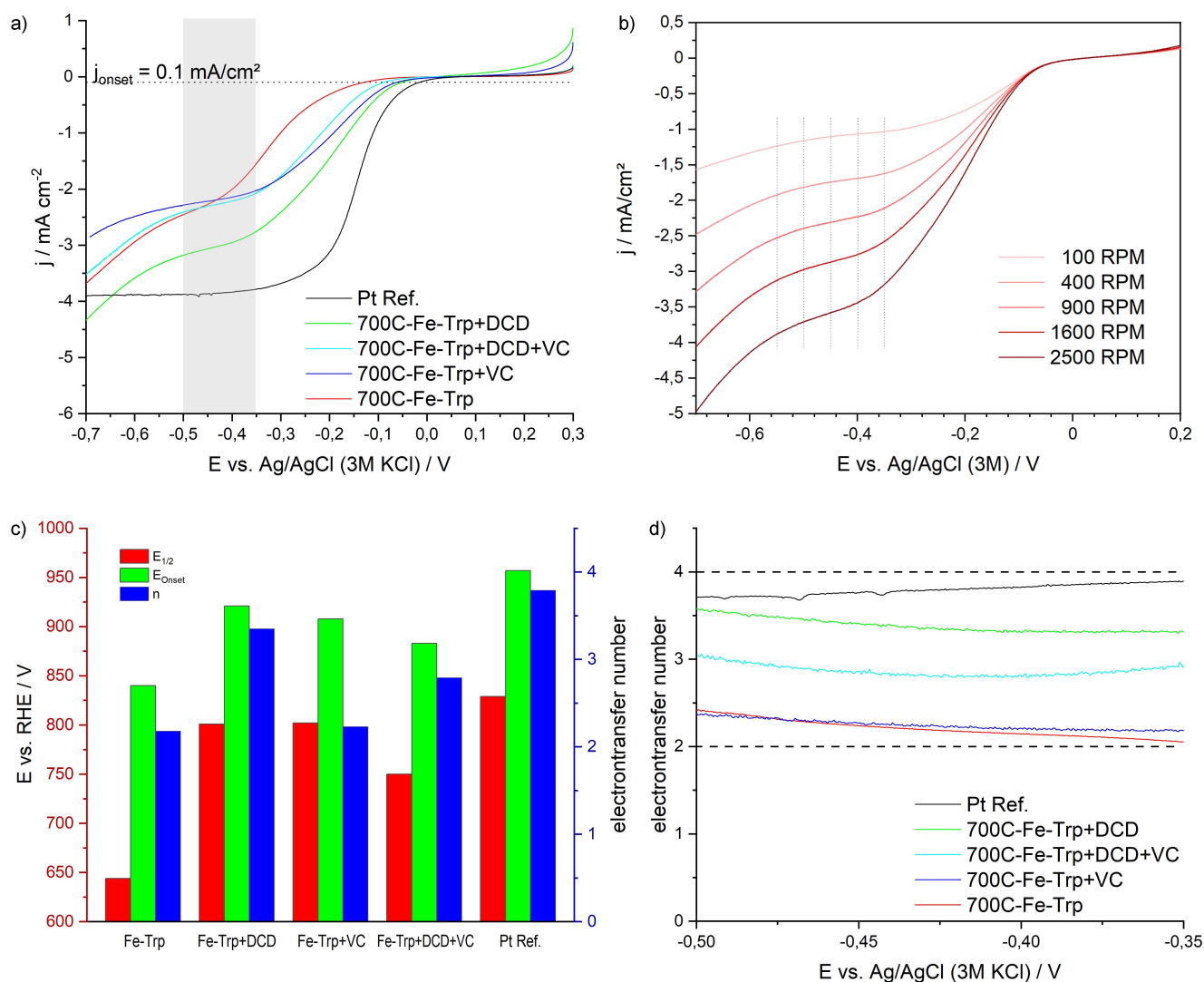
Figure 6. (a) LSVs of different catalysts at 1600 rpm in 0.1 M KOH measured vs. Ag/AgCl (3 M KCl) – dashed line showing the current density at the onset potential; (b) LSVs of Fe-Trp + DCD at various rotation rates; (c) Comparison chart of half-wave potential, onset potential, and electron transfer number of different catalysts; (d) electrontransfer numbers from Levich plots in the potential range marked by the grey box in (a).

based catalysts is well understood and follows a similar associative mechanism.[46] However, the binding energy of the [Pt]-OOH* transition state is higher compared to Fe-based catalysts, and Pt-based catalysts therefore usually show an electron transfer number close to 4. The electron transfer numbers of the herein tested catalysts indicate that a substantial amount of hydrogen peroxide is formed. The addition of DCD seems to suppress the H_2O_2 formation. This can be further investigated by rotating ring disk electrode (RRDE) experiments where the hydrogen peroxide that is formed at the catalyst film is oxidized under diffusion-controlled conditions at the ring and the ring current serves as a measure for the amount of H_2O_2 produced in the undesired 2-electron pathway.

3. Conclusions

We demonstrate a green synthesis pathway towards highly ORR active non-noble catalysts. The precursor is obtained from a solvent free mechanochemical approach using only non-toxic and readily available reactants. The low temperature carbonization at 700 °C gave electrocatalysts that demonstrated an electron transfer number of 3.4 in the ORR. These catalysts have shown to be a very promising alternative to PGM-based catalysts for the ORR in alkaline environments.

Future work will focus on the modification of these catalysts using fluorine with the intent of suppressing hydrogen peroxide generating side reactions. Furthermore, RDE experiments are carried out under conditions far from application and can only give a hint about a catalyst's performance. Therefore, the preparation of membrane electrode assemblies (MEA) and their

investigation in a realistic fuel cell setup are necessary to further evaluate the potential of these greener catalysts.

Acknowledgements

Conflict of Interest

The authors declare no conflict of interest.

[1] J. Rugolo, M. J. Aziz, *Energy Environ. Sci.* **2012**, *5*, 7151–7160.
[2] K. Qian, C. Zhou, M. Allan, Y. Yuan, in *2010 Int. Conf. Power Syst. Technol.*, IEEE, **2010**, pp. 1–6.
[3] A. Boudghene Stambouli, E. Traversa, *Renewable Sustainable Energy Rev.* **2002**, *6*, 297–306.
[4] Z. Chen, D. Higgins, A. Yu, L. Zhang, J. Zhang, *Energy Environ. Sci.* **2011**, *4*, 3167–3192.
[5] X. Ren, B. Liu, X. Liang, Y. Wang, Q. Lv, A. Liu, *J. Electrochem. Soc.* **2021**, *168*, 044521.
[6] Y. Sun, M. Delucchi, J. Ogden, *Int. J. Hydrogen Energy* **2011**, *36*, 11116–11127.
[7] C. J. Yang, *Energy Policy* **2009**, *37*, 1805–1808.
[8] Y. Shao, J. P. Dodelet, G. Wu, P. Zelenay, *Adv. Mater.* **2019**, *31*, 1807615.
[9] H. M. Barkholtz, D.-J. Liu, *Mater. Horiz.* **2017**, *4*, 20–37.
[10] U. Martinez, E. F. Holby, S. K. Babu, K. Artyushkova, L. Lin, S. Choudhury, G. M. Purdy, P. Zelenay, *J. Electrochem. Soc.* **2019**, *166*, F3136–F3142.
[11] L. Osmieri, A. H. A. Monteverde Videla, P. Ocón, S. Specchia, *J. Phys. Chem. C* **2017**, *121*, 17796–17817.
[12] R. Sgarbi, K. Kumar, F. Jaouen, A. Zitolo, E. A. Ticianelli, F. Maillard, *J. Solid State Electrochem.* **2021**, *25*, 45–56.
[13] M. M. Hossen, K. Artyushkova, P. Atanassov, A. Serov, *J. Power Sources* **2018**, *375*, 214–221.
[14] S. Gouse Peera, H. J. Kwon, T. G. Lee, A. M. Hussain, *Ionics* **2020**, *26*, 1563–1589.
[15] Y. Mun, S. Lee, K. Kim, S. Kim, S. Lee, J. W. Han, J. Lee, *J. Am. Chem. Soc.* **2019**, *141*, 6254–6262.
[16] S. S. A. Shah, T. Najam, M. K. Aslam, M. Ashfaq, M. M. Rahman, K. Wang, P. Tsiakaras, S. Song, Y. Wang, *Appl. Catal. B* **2020**, *268*, 118570.
[17] H. Zhang, S. Ding, S. Hwang, X. Zhao, D. Su, H. Xu, H. Yang, G. Wu, *J. Electrochem. Soc.* **2019**, *166*, F3116–F3122.
[18] R. Jasinski, *Nature* **1964**, *201*, 1212–1213.
[19] Y. Chen, I. Matanovic, E. Weiler, P. Atanassov, K. Artyushkova, *ACS Appl. Mater. Interfaces* **2018**, *1*, 5948–5953.
[20] J. Li, M. T. Sougrati, A. Zitolo, J. M. Ablett, I. C. Oğuz, T. Mineva, I. Matanovic, P. Atanassov, Y. Huang, I. Zenyuk, A. Di Cicco, K. Kumar, L. Dubau, F. Maillard, G. Dražić, F. Jaouen, *Nat. Catal.* **2021**, *4*, 10–19.

[21] X. Xu, Z. Xia, X. Zhang, R. Sun, X. Sun, H. Li, C. Wu, J. Wang, S. Wang, G. Sun, *Appl. Catal. B* **2019**, *259*, 118042.
[22] H. T. Chung, D. A. Cullen, D. Higgins, B. T. Sneed, E. F. Holby, K. L. More, P. Zelenay, *Science* **2017**, *357*, 479–484.
[23] K. Wiesener, *Electrochim. Acta* **1986**, *31*, 1073–1078.
[24] J. Sen Li, S. L. Li, Y. J. Tang, M. Han, Z. H. Dai, J. C. Bao, Y. Q. Lan, *Chem. Commun.* **2015**, *51*, 2710–2713.
[25] W.-J. Jiang, L. Gu, L. Li, Y. Zhang, X. Zhang, L.-J. Zhang, J.-Q. Wang, J.-S. Hu, Z. Wei, L.-J. Wan, *J. Am. Chem. Soc.* **2016**, *138*, 3570–3578.
[26] X. Yin, H. T. Chung, U. Martinez, L. Lin, K. Artyushkova, P. Zelenay, *J. Electrochem. Soc.* **2019**, *166*, F3240–F3245.
[27] J. Zhang, Q. Li, C. Zhang, L. Mai, M. Pan, S. Mu, *Electrochim. Acta* **2015**, *160*, 139–144.
[28] X. Wang, C. Yang, X. Wang, H. Zhu, L. Cao, A. Chen, L. Gu, Q. Zhang, L. Zheng, H. P. Liang, *ACS Sustainable Chem. Eng.* **2021**, *9*, 137–146.
[29] R. Karunagaran, C. Coghlan, C. Shearer, D. Tran, K. Gulati, T. T. Tung, C. Doonan, D. Losic, *Materials (Basel).* **2018**, *11*, DOI 10.3390/ma11020205.
[30] US Department of Agriculture, Agricultural Research Service, Nutrient Data Laboratory, **2016**.
[31] M. Klimakow, P. Klobes, A. F. Thünemann, K. Rademann, F. Emmerling, *Chem. Mater.* **2010**, *22*, 5216–5221.
[32] S. L. James, C. J. Adams, C. Bolm, D. Braga, P. Collier, T. Frisčˇ, F. Frisčˇic', F. Grepioni, K. D. M. Harris, G. Hyett, W. Jones, A. Krebs, J. Mack, L. Maini, A. G. Orpen, I. P. Parkin, W. C. Shearouse, J. W. Steed, D. C. Waddell, *Chem. Soc. Rev.* **2012**, *41*, 413–447.
[33] A. A. Van Der Giessen, *Chemical and Physical Properties of Iron (III)-Oxide Hydrate*, Technische Hogeschool te Eindhoven, **1968**.
[34] T. Degen, M. Sadki, E. Bron, U. König, G. Nénert, *Powder Diffr.* **2014**, *29*, S13–S18.
[35] K. Lagarec, D. G. Rancourt, Recoil, mössbauer spectral analysissoftware for windows 1.0, Department of Physics, University of Ottawa, Canada **1998**.
[36] T. Tsuzuki, P. G. Mccormick, *J. Mater. Sci.* **2004**, *39*, 5143–5146.
[37] DOE Durability Working Group, *Rotating Disk-Electrode Aqueous Electrolyte Accelerated Stress Tests for PGM Electrocatalyst/ Support Durability Evaluation*, **2011**.
[38] S. C. F. Au-Yeung, G. Denes, J. E. Greedan, D. R. Eaton, T. Birchall, *Inorg. Chem.* **1984**, *23*, 1513–1517.
[39] W. D. Birch, A. Pring, A. Reller, H. W. Schmalle, *Am. Mineral.* **1993**, *78*, 827–834.
[40] X. W. Liu, S. Zhao, Y. Meng, Q. Peng, A. K. Dearden, C. F. Huo, Y. Yang, Y. W. Li, X. D. Wen, *Sci. Rep.* **2016**, *6*.
[41] U. I. Kramm, M. Lefèvre, N. Larouche, D. Schmeisser, J. P. Dodelet, *J. Am. Chem. Soc.* **2014**, *136*, 978–985.
[42] U. I. Kramm, L. Ni, S. Wagner, *Adv. Mater.* **2019**, *31*, 1–11.
[43] M. Xiao, J. Zhu, L. Ma, Z. Jin, J. Ge, X. Deng, Y. Hou, Q. He, J. Li, Q. Jia, S. Mukerjee, R. Yang, Z. Jiang, D. Su, C. Liu, W. Xing, *ACS Catal.* **2018**, *8*, 2824–2832.
[44] Y. Ye, L. Zhang, Q. Peng, G.-E. E. Wang, Y. Shen, Z. Li, L. Wang, X. Ma, Q.-H. H. Chen, Z. Zhang, S. Xiang, *J. Am. Chem. Soc.* **2015**, *137*, 913–918.
[45] Y. Hou, T. Huang, Z. Wen, S. Mao, S. Cui, J. Chen, *Adv. Energy Mater.* **2014**, *4*, 1400337.
[46] J. Greeley, N. M. Markovic, *Energy Environ. Sci.* **2012**, *5*, 9246–9256.